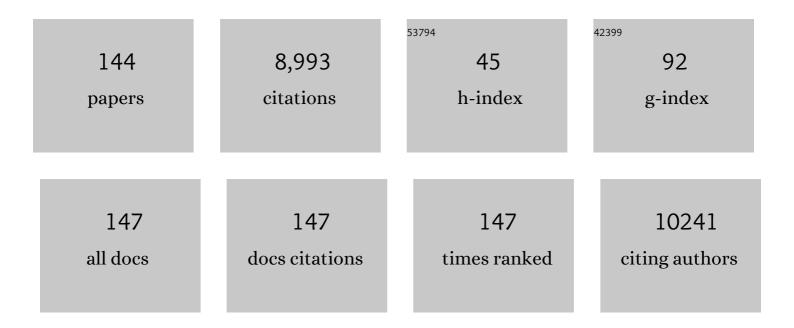
Binghui Ge

List of Publications by Year in descending order

Source: https://exaly.com/author-pdf/5492380/publications.pdf Version: 2024-02-01



RINCHUL CE

#	Article	IF	CITATIONS
1	Atomically dispersed platinum supported on curved carbon supports for efficient electrocatalytic hydrogen evolution. Nature Energy, 2019, 4, 512-518.	39.5	756
2	Tuning defects in oxides at roomÂtemperature by lithium reduction. Nature Communications, 2018, 9, 1302.	12.8	428
3	Tuning the Selectivity of Catalytic Carbon Dioxide Hydrogenation over Iridium/Cerium Oxide Catalysts with a Strong Metal–Support Interaction. Angewandte Chemie - International Edition, 2017, 56, 10761-10765.	13.8	384
4	Tellurium as a high-performance elemental thermoelectric. Nature Communications, 2016, 7, 10287.	12.8	369
5	Lattice Dislocations Enhancing Thermoelectric PbTe in Addition to Band Convergence. Advanced Materials, 2017, 29, 1606768.	21.0	365
6	Vacancy-induced dislocations within grains for high-performance PbSe thermoelectrics. Nature Communications, 2017, 8, 13828.	12.8	360
7	Lattice Strain Advances Thermoelectrics. Joule, 2019, 3, 1276-1288.	24.0	333
8	Iced photochemical reduction to synthesize atomically dispersed metals by suppressing nanocrystal growth. Nature Communications, 2017, 8, 1490.	12.8	322
9	Promoting SnTe as an Ecoâ€Friendly Solution for pâ€PbTe Thermoelectric via Band Convergence and Interstitial Defects. Advanced Materials, 2017, 29, 1605887.	21.0	317
10	A versatile route to fabricate single atom catalysts with high chemoselectivity and regioselectivity in hydrogenation. Nature Communications, 2019, 10, 3663.	12.8	270
11	Interstitial Point Defect Scattering Contributing to High Thermoelectric Performance in SnTe. Advanced Electronic Materials, 2016, 2, 1600019.	5.1	235
12	Low Sound Velocity Contributing to the High Thermoelectric Performance of Ag ₈ SnSe ₆ . Advanced Science, 2016, 3, 1600196.	11.2	215
13	Band and scattering tuning for high performance thermoelectric Sn1â~'xMnxTe alloys. Journal of Materiomics, 2015, 1, 307-315.	5.7	193
14	Atomic Cobalt Covalently Engineered Interlayers for Superior Lithiumâ€Ion Storage. Advanced Materials, 2018, 30, e1802525.	21.0	187
15	Ti ₃ C ₂ T _{<i>x</i>} MXene-Based Flexible Piezoresistive Physical Sensors. ACS Nano, 2022, 16, 1734-1758.	14.6	177
16	Atomic-level structure engineering of metal oxides for high-rate oxygen intercalation pseudocapacitance. Science Advances, 2018, 4, eaau6261.	10.3	164
17	Boosting the thermoelectric performance of PbSe through dynamic doping and hierarchical phonon scattering. Energy and Environmental Science, 2018, 11, 1848-1858.	30.8	163
18	Threeâ€Dimensional Hierarchical Architectures Constructed by Graphene/MoS ₂ Nanoflake Arrays and Their Rapid Charging/Discharging Properties as Lithiumâ€Ion Battery Anodes. Chemistry - A European Journal, 2013, 19, 5818-5823.	3.3	141

#	Article	IF	CITATIONS
19	Ultrahigh thermoelectric performance in Cu 2â^'y Se 0.5 S 0.5 liquid-like materials. Materials Today Physics, 2017, 1, 14-23.	6.0	130
20	Significant Role of Mg Stoichiometry in Designing High Thermoelectric Performance for Mg ₃ (Sb,Bi) ₂ -Based n-Type Zintls. Journal of the American Chemical Society, 2018, 140, 1910-1915.	13.7	125
21	â^'60 °C solution synthesis of atomically dispersed cobalt electrocatalyst with superior performance. Nature Communications, 2019, 10, 606.	12.8	121
22	Synergistic effect of an atomically dual-metal doped catalyst for highly efficient oxygen evolution. Journal of Materials Chemistry A, 2018, 6, 6840-6846.	10.3	113
23	Synthesis of NiMo catalysts supported on mesoporous Al2O3 with different crystal forms and superior catalytic performance for the hydrodesulfurization of dibenzothiophene and 4,6-dimethyldibenzothiophene. Journal of Catalysis, 2016, 344, 680-691.	6.2	111
24	In situ trapped high-density single metal atoms within graphene: Iron-containing hybrids as representatives for efficient oxygen reduction. Nano Research, 2018, 11, 2217-2228.	10.4	108
25	Short-range order in defective half-Heusler thermoelectric crystals. Energy and Environmental Science, 2019, 12, 1568-1574.	30.8	86
26	Tuning the Selectivity of Catalytic Carbon Dioxide Hydrogenation over Iridium/Cerium Oxide Catalysts with a Strong Metal–Support Interaction. Angewandte Chemie, 2017, 129, 10901-10905.	2.0	83
27	Pure Siliceous Zeolite-Supported Ru Single-Atom Active Sites for Ammonia Synthesis. Chemistry of Materials, 2019, 31, 9413-9421.	6.7	83
28	Elucidating the Copper–HÃ g g Iron Carbide Synergistic Interactions for Selective CO Hydrogenation to Higher Alcohols. ACS Catalysis, 2017, 7, 5500-5512.	11.2	82
29	Ultralow-temperature photochemical synthesis of atomically dispersed Pt catalysts for the hydrogen evolution reaction. Chemical Science, 2019, 10, 2830-2836.	7.4	82
30	Thermoelectric Enhancements in PbTe Alloys Due to Dislocationâ€Induced Strains and Converged Bands. Advanced Science, 2020, 7, 1902628.	11.2	78
31	Scalable Synthesis of 2D Si Nanosheets. Advanced Materials, 2017, 29, 1701777.	21.0	77
32	Phonon scattering by nanoscale twin boundaries. Nano Energy, 2017, 32, 174-179.	16.0	77
33	Boosting the Electrocatalytic Water Oxidation Performance of CoFe ₂ O ₄ Nanoparticles by Surface Defect Engineering. ACS Applied Materials & Interfaces, 2019, 11, 3978-3983.	8.0	76
34	Cu Interstitials Enable Carriers and Dislocations for Thermoelectric Enhancements in n-PbTe0.75Se0.25. CheM, 2020, 6, 523-537.	11.7	69
35	High Thermoelectric Performance of New Rhombohedral Phase of GeSe stabilized through Alloying with AgSbSe ₂ . Angewandte Chemie - International Edition, 2017, 56, 14113-14118.	13.8	68
36	Distribution of rhenium in a single crystal nickel-based superalloy. Scripta Materialia, 2010, 63, 969-972.	5.2	67

#	Article	IF	CITATIONS
37	Scalable shear-exfoliation of high-quality phosphorene nanoflakes with reliable electrochemical cycleability in nano batteries. 2D Materials, 2016, 3, 025005.	4.4	66
38	Visualizing the Electrochemical Lithiation/Delithiation Behaviors of Black Phosphorus by <i>in Situ</i> Transmission Electron Microscopy. Journal of Physical Chemistry C, 2016, 120, 5861-5868.	3.1	65
39	Atomic species derived CoOx clusters on nitrogen doped mesoporous carbon as advanced bifunctional electro-catalysts for Zn-air battery. Energy Storage Materials, 2020, 29, 156-162.	18.0	62
40	Direct immobilization of an atomically dispersed Pt catalyst by suppressing heterogeneous nucleation at â^'40 °C. Journal of Materials Chemistry A, 2019, 7, 25779-25784.	10.3	61
41	Monodisperse Molybdenum Nanoparticles as Highly Efficient Electrocatalysts for Li-S Batteries. ACS Nano, 2021, 15, 15047-15056.	14.6	60
42	Crystal-plane effects of MFI zeolite in catalytic conversion of methanol to hydrocarbons. Journal of Catalysis, 2018, 360, 89-96.	6.2	58
43	In situ TEM probing of crystallization form-dependent sodiation behavior in ZnO nanowires for sodium-ion batteries. Nano Energy, 2016, 30, 771-779.	16.0	57
44	Single-Atom Electroplating on Two Dimensional Materials. Chemistry of Materials, 2019, 31, 429-435.	6.7	55
45	lce as Solid Electrolyte To Conduct Various Kinds of Ions. Angewandte Chemie - International Edition, 2019, 58, 12569-12573.	13.8	54
46	Surface Engineering of Perovskite Oxide for Bifunctional Oxygen Electrocatalysis. Small Methods, 2019, 3, 1800279.	8.6	47
47	Constructing Graphiticâ€Nitrogenâ€Bonded Pentagons in Interlayerâ€Expanded Graphene Matrix toward Carbonâ€Based Electrocatalysts for Acidic Oxygen Reduction Reaction. Advanced Materials, 2021, 33, e2103133.	21.0	47
48	Revealing the role of lattice distortions in the hydrogen-induced metal-insulator transition of SmNiO3. Nature Communications, 2019, 10, 694.	12.8	46
49	Study of microstructure of nickel-based superalloys at high temperatures. Scripta Materialia, 2017, 126, 55-57.	5.2	45
50	Overcoming synthetic metastabilities and revealing metal-to-insulator transition & thermistor bi-functionalities for d-band correlation perovskite nickelates. Materials Horizons, 2019, 6, 788-795.	12.2	44
51	Substitutions and dislocations enabled extraordinary n-type thermoelectric PbTe. Materials Today Physics, 2021, 17, 100355.	6.0	44
52	Confining Zeroâ€Valent Platinum Single Atoms in αâ€MoC _{1â~'} <i>_x</i> for pHâ€Universal Hydrogen Evolution Reaction. Advanced Functional Materials, 2022, 32, 2108464.	14.9	43
53	Atom-Thin SnS2–xSex with Adjustable Compositions by Direct Liquid Exfoliation from Single Crystals. ACS Nano, 2016, 10, 755-762.	14.6	39
54	High-metallic-phase-concentration Mo1–xWxS2 nanosheets with expanded interlayers as efficient electrocatalysts. Nano Research, 2018, 11, 1687-1698.	10.4	37

#	Article	IF	CITATIONS
55	Ice Melting to Release Reactants in Solution Syntheses. Angewandte Chemie - International Edition, 2018, 57, 3354-3359.	13.8	36
56	Epitaxy of Ultrathin SnSe Single Crystals on Polydimethylsiloxane: Inâ€Plane Electrical Anisotropy and Gateâ€Tunable Thermopower. Advanced Electronic Materials, 2016, 2, 1600292.	5.1	31
57	Defect-Laden MoSe ₂ Quantum Dots Made by Turbulent Shear Mixing as Enhanced Electrocatalysts. Small, 2017, 13, 1700565.	10.0	31
58	Thermoelectric performance enhancement of Mg ₂ Sn based solid solutions by band convergence and phonon scattering via Pb and Si/Ge substitution for Sn. Physical Chemistry Chemical Physics, 2016, 18, 20726-20737.	2.8	30
59	Self-compensation induced vacancies for significant phonon scattering in InSb. Nano Energy, 2018, 48, 189-196.	16.0	30
60	Triggering electronic coupling between neighboring hetero-diatomic metal sites promotes hydrogen evolution reaction kinetics. Nano Energy, 2022, 98, 107296.	16.0	30
61	Restraining the Band Fluctuation of CBDâ€Zn(O,S) Layer: Modifying the Heteroâ€Junction Interface for High Performance Cu ₂ ZnSnSe ₄ Solar Cells With Cdâ€Free Buffer Layer. Solar Rrl, 2017, 1, 1700075.	5.8	29
62	Role of Ru Oxidation Degree for Catalytic Activity in Bimetallic Pt/Ru Nanoparticles. Journal of Physical Chemistry C, 2016, 120, 6569-6576.	3.1	25
63	Intrinsically Low Lattice Thermal Conductivity in Natural Superlattice (Bi ₂) _{<i>m</i>} (Bi ₂ Te ₃) _{<i>m</i>} Thermoelectric Materials. Chemistry of Materials, 2021, 33, 1140-1148.	6.7	25
64	Catalyst-free growth of nanocrystalline graphene/graphite patterns from photoresist. Chemical Communications, 2013, 49, 2789.	4.1	24
65	Competing Interfacial Reconstruction Mechanisms in La _{0.7} Sr _{0.3} MnO ₃ /SrTiO ₃ Heterostructures. ACS Applied Materials & Interfaces, 2016, 8, 24192-24197.	8.0	24
66	In situ TEM visualization of superior nanomechanical flexibility of shear-exfoliated phosphorene. Nanoscale, 2016, 8, 13603-13610.	5.6	23
67	In Situ Constructing the Kinetic Roadmap of Octahedral Nanocrystal Assembly Toward Controlled Superlattice Fabrication. Journal of the American Chemical Society, 2021, 143, 4234-4243.	13.7	23
68	Manipulation of Band Degeneracy and Lattice Strain for Extraordinary PbTe Thermoelectrics. Research, 2020, 2020, 8151059.	5.7	23
69	Active {010} facet-exposed Cu2MoS4 nanotube as high-efficiency photocatalyst. Nano Research, 2017, 10, 3817-3825.	10.4	22
70	Ultrahigh Thermoelectric Performance in SrNb _{0.2} Ti _{0.8} O ₃ Oxide Films at a Submicrometer-Scale Thickness. ACS Energy Letters, 2017, 2, 915-921.	17.4	21
71	Characterization of a-plane InN film grown on r-plane sapphire by MOCVD. Journal of Crystal Growth, 2008, 310, 3726-3729.	1.5	20
72	Study of γ/γ′ Interfaces in Nickel-Based, Single-Crystal Superalloys by Scanning Transmission Electron Microscopy. Metallurgical and Materials Transactions A: Physical Metallurgy and Materials Science, 2011, 42, 548-552.	2.2	20

#	Article	IF	CITATIONS
73	Effect of the degree of dispersion of Pt over MgAl 2 O 4 on the catalytic hydrogenation of benzaldehyde. Chinese Journal of Catalysis, 2017, 38, 1613-1620.	14.0	20
74	Na-doping enables both dislocations and holes in EuMg ₂ Sb ₂ for thermoelectric enhancements. Journal of Materials Chemistry A, 2020, 8, 8345-8351.	10.3	20
75	ZnAl ₂ O ₄ Spinel-Supported PdZn _β Catalyst with Parts per Million Pd for Methanol Steam Reforming. ACS Catalysis, 2022, 12, 2714-2721.	11.2	20
76	High Thermoelectric Performance of New Rhombohedral Phase of GeSe stabilized through Alloying with AgSbSe ₂ . Angewandte Chemie, 2017, 129, 14301-14306.	2.0	19
77	General Strategy for Two-Dimensional Transition Metal Dichalcogenides by Ion Exchange. Chemistry of Materials, 2017, 29, 10019-10026.	6.7	18
78	Tungsten Nanoparticles Accelerate Polysulfides Conversion: A Viable Route toward Stable Roomâ€īemperature Sodium–Sulfur Batteries. Advanced Science, 2022, 9, e2105544.	11.2	18
79	Ultrathin two-dimensional metals with fully exposed (111) facets. Chemical Communications, 2018, 54, 160-163.	4.1	17
80	Beyond conventional sodium-ion storage mechanisms: a combinational intercalation/conversion reaction mechanism in Ni-ion modified hydrated vanadate for high-rate sodium-ion storage. Energy Storage Materials, 2022, 47, 579-590.	18.0	17
81	Wet-milling synthesis of immobilized Pt/Ir nanoclusters as promising heterogeneous catalysts. Nano Research, 2022, 15, 3065-3072.	10.4	17
82	Overlooked Transportation Anisotropies in d-Band Correlated Rare-Earth Perovskite Nickelates. Matter, 2020, 2, 1296-1306.	10.0	16
83	Crystal symmetry enables high thermoelectric performance of rhombohedral GeSe(MnCdTe2). Nano Energy, 2022, 100, 107434.	16.0	16
84	Study of γ/γ′ interfacial width in a nickel-based superalloy by scanning transmission electron microscopy. Philosophical Magazine Letters, 2012, 92, 541-546.	1.2	15
85	Ice Melting to Release Reactants in Solution Syntheses. Angewandte Chemie, 2018, 130, 3412-3417.	2.0	15
86	Charge-Transfer-Induced Photoluminescence Properties of WSe ₂ Monolayer–Bilayer Homojunction. ACS Applied Materials & Interfaces, 2019, 11, 20566-20573.	8.0	15
87	Ultralow lattice thermal conductivity enables high thermoelectric performance in BaAg2Te2 alloys. Materials Today Physics, 2022, 22, 100591.	6.0	14
88	A review of sample thickness effects on high-resolution transmission electron microscopy imaging. Micron, 2020, 130, 102813.	2.2	13
89	Sublattice Short-Range Order and Modified Electronic Structure in Defective Half-Heusler Nb _{0.8} CoSb. Journal of Physical Chemistry C, 2021, 125, 1125-1133.	3.1	13
90	Atomic Mechanism of Hybridization-Dependent Surface Reconstruction with Tailored Functionality in Hexagonal Multiferroics. ACS Applied Materials & amp; Interfaces, 2017, 9, 27322-27331.	8.0	12

#	Article	IF	CITATIONS
91	<i>In situ</i> growth of ZnO/SnO ₂ (ZnO:Sn) _m binary/superlattice heterojunction nanowire arrays. CrystEngComm, 2018, 20, 556-562.	2.6	12
92	A Unique Ru-N ₄ -P Coordinated Structure Synergistically Waking Up the Nonmetal P Active Site for Hydrogen Production. Research, 2020, 2020, 5860712.	5.7	12
93	Microscopic study of thermoelectric In-doped SnTe. Nanotechnology, 2018, 29, 26LT01.	2.6	11
94	Visualizing Tailored Spin Phenomena in a Reducedâ€Đimensional Topological Superlattice. Advanced Materials, 2020, 32, e2005315.	21.0	11
95	A New Ferroelectric Phase of <scp><scp>YMnO</scp></scp> ₃ Induced by Oxygenâ€Vacancy Ordering. Journal of the American Ceramic Society, 2014, 97, 1264-1268.	3.8	10
96	Direct observation of interlocked domain walls and topological four-state vortex-like domain patterns in multiferroic YMnO3 single crystal. Applied Physics Letters, 2015, 106, .	3.3	10
97	Direct observation of incommensurate charge-density wave in overdoped manganites. Materials Today Physics, 2018, 5, 7-11.	6.0	10
98	Ice as Solid Electrolyte To Conduct Various Kinds of Ions. Angewandte Chemie, 2019, 131, 12699-12703.	2.0	10
99	Manipulation of Defects for Highâ€Performance Thermoelectric PbTeâ€Based Alloys. Small Structures, 2021, 2, 2100016.	12.0	10
100	Growth, conductivity and periodic poled structure of doped KTiOPO4 and its analogue crystals. Optical Materials, 2006, 28, 355-359.	3.6	9
101	Near ultraviolet InGaN/GaN MQWs grown on maskless periodically grooved sapphire substrates fabricated by wet chemical etching. Journal of Alloys and Compounds, 2007, 428, 312-315.	5.5	9
102	Determining polarity and dislocation core structures at atomic level for epitaxial AlN/(0 0 0 1)6H-SiC from a single image in HRTEM. Ultramicroscopy, 2013, 126, 77-84.	1.9	9
103	Growth, conductivity and generation of blue coherent laser of cesium doped KTiOPO4 crystals. Journal of Crystal Growth, 2004, 267, 517-521.	1.5	8
104	STEM image simulation with hybrid CPU/GPU programming. Ultramicroscopy, 2016, 166, 1-8.	1.9	8
105	Improved thermoelectric performance in p-type Bi 0.48 Sb 1.52 Te 3 bulk material by adding MnSb 2 Se 4. Chinese Physics B, 2017, 26, 017202.	1.4	8
106	Direct visualization of spatially correlated displacive short-range ordering in Nb _{0.8} CoSb. Nanoscale, 2020, 12, 21624-21628.	5.6	8
107	ZnS/Zn2SnO4 biaxial nanowire heterostructures. Physica E: Low-Dimensional Systems and Nanostructures, 2010, 42, 1435-1440.	2.7	7
108	Preparation and properties of functionalized graphene/waterborne polyurethane composites with highly hydrophobic. Journal of Applied Polymer Science, 2015, 132, .	2.6	7

#	Article	IF	CITATIONS
109	Filling fraction of Yb in CoSb3 Skutterudite studied by electron microscopy. Applied Physics Letters, 2017, 110, .	3.3	7
110	Frequency switchable correlated transports in perovskite rare-earth nickelates. Journal of Materials Chemistry A, 2020, 8, 13630-13637.	10.3	7
111	Isomeric Compound Dendrites on a Monolayer WS ₂ Substrate: Morphological Engineering and Formation Mechanism. ACS Applied Nano Materials, 2021, 4, 8408-8416.	5.0	7
112	Exploration of the bond angle and charge carrier density by rare-earth doping in <mml:math xmlns:mml="http://www.w3.org/1998/Math/MathML"><mml:mrow><mml:msub><mml:mi>Sr</mml:mi><mml:m Physical Review Materials, 2020, 4, .</mml:m </mml:msub></mml:mrow></mml:math 	n <i>%</i> 24/mm	l:m/n>
113	Determination of the incommensurate modulated structure of Bi2Sr1.6La0.4CuO6+ by aberration-corrected transmission electron microscopy. Ultramicroscopy, 2015, 159, 67-72.	1.9	6
114	Delta-temperatural electronic transportation achieved in metastable perovskite rare-earth nickelate thin films. Journal of Materials Chemistry C, 2019, 7, 8101-8108.	5.5	6
115	Artificial Second-Order Nonlinear Optics in a Centrosymmetric Optical Material BiVO ₄ : Breaking the Prerequisite for Nonlinear Optical Materials. ACS Omega, 2019, 4, 1045-1052.	3.5	6
116	Synthesis and characterization of high-purity SnO ₂ (ZnO:Sn) _m superlattice nanowire arrays with broad-spectrum emissions. CrystEngComm, 2020, 22, 5355-5362.	2.6	6
117	Study of Point Spread in the Aberration-Corrected Transmission Electron Microscopy. Microscopy and Microanalysis, 2014, 20, 1447-1452.	0.4	5
118	Visualizing Emergent Magnetic Flux of Antiskyrmions in Mn _{1.4} PtSn Magnet. Advanced Functional Materials, 2022, 32, .	14.9	5
119	Nucleation growth quenching for superior cluster catalysts. Nano Research, 2022, 15, 7933-7939.	10.4	5
120	Investigation of non-linear imaging in high-resolution transmission electron microscopy. Microscopy (Oxford, England), 2016, 65, 465-472.	1.5	4
121	Investigations of atomic configurations of 60° basal dislocations in wurtzite GaN film by high-resolution transmission electron microscopy. Philosophical Magazine Letters, 2016, 96, 148-156.	1.2	4
122	Applicability of non-linear imaging in high-resolution transmission electron microscopy. Journal of Electron Microscopy, 2017, 66, 406-413.	0.9	4
123	Enhancement of Interfacial Polarization in BaTiO 3 Thin Films via Oxygen Inhomogeneity. Advanced Electronic Materials, 0, , 2100876.	5.1	4
124	A study of one-dimensional incommensurate modulated structure determination in high-resolution transmission electron microscopy. Acta Crystallographica Section A: Foundations and Advances, 2014, 70, 563-571.	0.1	3
125	Solution-processed anchoring zinc oxide quantum dots on covalently modified graphene oxide. Journal of Nanoparticle Research, 2014, 16, 1.	1.9	3
126	Insight into long-period pattern by depth sectioning using aberration-corrected scanning transmission electron microscope. Ultramicroscopy, 2020, 209, 112885.	1.9	3

#	Article	IF	CITATIONS
127	Revealing the origin of dislocations in Pb _{1â^'x} Sb _{2x/3} Se (0 < <i>x</i> ≤0.07). Nanoscale, 2020, 12, 19165-19169.	5.6	3
128	Wafer-scale metal chalcogenide thin films <i>via</i> an ion exchange approach. Journal of Materials Chemistry C, 2020, 8, 14393-14401.	5.5	3
129	Phase junction-confined single-atom TiO ₂ –Pt ₁ –CeO ₂ for multiplying catalytic oxidation efficiency. Catalysis Science and Technology, 2021, 11, 4650-4657.	4.1	3
130	Characterization of metal-organic frameworks by transmission electron microscopy. Advances in Physics: X, 2022, 7, .	4.1	3
131	Atomic resolution imaging of oxygen atoms close to heavy atoms by HRTEM and ED, using the superconductor SmFeAsO0.85F0.15 as an example. Micron, 2015, 71, 32-38.	2.2	2
132	Electronic and lattice structure of CaFe1â^'xCoxAsF probed by x-ray absorption spectroscopy. Materials Research Express, 2020, 7, 016001.	1.6	2
133	Fast determination of sample thickness through scanning moir \tilde{A} \mbox{C} fringes in scanning transmission electron microscopy. Micron, 2022, 155, 103230.	2.2	2
134	Short-range ordering of heavy-element columns in nickel-based superalloys. Philosophical Magazine Letters, 2016, 96, 432-439.	1.2	1
135	Innenrücktitelbild: Ice Melting to Release Reactants in Solution Syntheses (Angew. Chem. 13/2018). Angewandte Chemie, 2018, 130, 3579-3579.	2.0	1
136	Scanning Transmission Electron Microscopy (STEM). Springer Tracts in Modern Physics, 2018, , 205-254.	0.1	1
137	Further discussion on the separation of linear and nonlinear components in HRTEM imaging. Micron, 2021, 145, 103054.	2.2	1
138	<i>In Situ</i> Investigation of the Phase Transition at the Surface of Thermoelectric PbTe with van der Waals Control. Research, 2022, 2022, 9762401.	5.7	1
139	A dynamical Lie algebraic treatment for the optical nonlinearity of disubstituted benzenes. Chemical Physics, 2003, 287, 21-32.	1.9	0
140	Interfaces in La1.89Ce0.11CuO4/Ba0.5Sr0.5TiO3/La0.88Sr0.12MnO3heterostructures on (0 0 1) SrTiO3substrates. Philosophical Magazine Letters, 2014, 94, 205-210.	1.2	0
141	Mapping Valence Electron Distribution of Iron-Based Superconductors using Quantitative CBED and Precession Electron Diffraction. Microscopy and Microanalysis, 2015, 21, 1099-1100.	0.4	0
142	Roles of Oxygen Vacancy in Improper Ferroelectrics. Microscopy and Microanalysis, 2018, 24, 74-75.	0.4	0
143	Rational design for high-yield monolayer WS2 films in confined space under fast thermal processing. Nanotechnology, 2021, 32, 505603.	2.6	0
144	Novel SnO2(ZnO:Sn)m superlattice nanoparticles for ultra-low ppb-level H2S detection. CrystEngComm, 0, , .	2.6	0